Green synthesis of emerging ZnO and Ca-doped ZnO nanoparticles towards optical, magnetic properties and its antibacterial application

R. Revathi[a], S. Revathi[b], R. Jothiramalingam[c,*], M. Sukumar[d], N. Mohamed Basith[e], M. Sundararajan[f,*], S. Yuvaraj[g], S. Arokiyraj[h]

[a]*Department of Biotechnology, Periyar University Centre for Post Graduate and Research Studies, Dharmapuri, 635 205, India.*
[b]*School of Electronics Engineering, Vellore Institute of Technology (VIT), Chennai 600 127, India.*
[c]*Department of chemistry, College of science, King Saud University, P.O. Box 2455, Riyadh 11451, Saudi Arabia.*
[d]*Department of Applied Physics, Sri Venkateswara College of Engineering, Sriperumbudur 602 117, Tamil Nadu, India*
[e]*Post-Graduate and Research Department of Chemistry, The New College (Autonomous), University of Madras, Chennai, 600014, India*
[f]*PG & Research Department of Physics, Paavendhar College of Arts & Science, M.V. South, Thalaivasal, Salem 636 121,Tamilnadu, India*
[g]*Department of Physics, Vel Tech Rangarajan Dr. Sagunthala R&D Institute of Science and Technology, Chennai 600 062,Tamilnadu, India*
[h]*Department of Food Science and Biotechnology, Sejong University, Gwangjin-gu, Seoul -05006, South Korea.*

A green synthesis method is adopted to prepare emerging low cost ZnO (ZNP) and Ca substitute ZnO nanoparticles (CZNP) using Psidium guajava fruit (PGF) extract as an effective reducing and capping agent. An X-ray diffraction study of the synthesized nanoparticles revealed that they have a hexagonal wurtzite structure. The elemental compositions and oxidation states of ZNP and CZNP surfaces are quantified. The HR-SEM image shows the nano-flake like structure of the synthesized nanomaterials ZNP and CZNP samples. The elemental compositions were identified using EDAX spectra. From the Raman spectra, the low wavenumber region of 2nd order Raman modes at 341 and 346 cm^{-1} were ascribed to the difference E_2^{high}-E_2^{low}. Kubelka–Munk (K–M) method is used for estimating direct band gap and it is 3.3 eV and 3.04 eV for ZNP and CZNP respectively. Due to the zinc and oxygen vacancies, six different bands were observed in the photoluminescence spectra. The TG analysis was observed 5.6% of weight loss for ZNP and 5.8% of weight loss for CZNP sample. The Magnetization–Field (M–H) hysteresis curves revealed the appearance of diamagnetic behavior at room temperature. The as-fabricated pure ZnO and Ca-doped ZnO nanoparticles were evaluated for the antibacterial activity. The Ca substituted ZnO sample showed higher antibacterial activity than pure ZnO sample.

(Received September 11, 2023; Accepted December 15, 2023)

Keywords: Green synthesis, surface chemistry, Optical property, Raman spectrum, Antibacterial activity

1. Introduction

Nanoparticles have attracted a lot of attention recently in a variety of applications as it has unique structural, optical, surface and magnetic properties as compared to their bulk compounds. ZnO nanomaterial have wide direct band gap of 3.36 eV and large exciton binding energy of 60 meV and it is suitable material for various applications in spintronics, catalysis, sensors,

* Corresponding authors: jrajabathar@ksu.edu.sa
https://doi.org/10.15251/DJNB.2023.184.1587

semiconductor device [1-7], cosmetic colorings matter, SAW equipment fabrication, electrical resistance, optical materials, heterogeneous catalyst, UV radiation absorbers, and window layers of solar cells [8], OLEDs [9], lasers and antibacterial activities. Researchers explore the unique properties of ZnO for the above mentioned applications and its electrical and optical properties can be further improved by doping with metal elements. ZnO doped with metal elements is widely used for fabrication of optoelectronic devices [10]. In early literature, Geetha Devi et al. (2016) and Umaralikhan et al. (2017) showed that the optical behavior of the core material could be enhanced by reducing the defect level through the dopant [11, 12, 13, 14, 15].

Nanoparticles are synthesized by various methods. Among the various methods, we concentrate on the eco-friendly green synthesis method. The green synthesis technique is a promising and eco-friendly method [14].In green synthesis, we prefer Psidiumguajava fruit (PGF) extract to synthesize nanoparticles. Vitamin A, C, iron, phosphorus, calcium, saponin, oleanolic acid, morin-3-O-L-lyxopyranoside, morin-3-O-L-arabopyranoside, guaijavarin, quercetin, and flavonoids are all found in PGF skin [15, 16].Cancerous cell curing and ageing skin in young people can be prevented through the phenolic compounds of PGF.

In the present work to prepare ZnO and Ca substitute ZnO nanoparticles were fabricated using PGF extract as a reducing and capping mediator by the eco-friendly green synthesis. The fabricated materials were investigated by structural, optical, and thermal properties zinc oxide and calcium doped zinc oxide materials. In optical observance, results show a defect level reduction on CZNP and ZNP samples, the CZNP sample shows the maximum optical properties. The as-fabricated CZNPs were then investigated for antibacterial activity to determine potential applications for them in the future.

2. Experimental

2.1. Preparation of Psidiumguajava fruit (PGF) extracts

25g of fresh little bits of PGF were added to 200 ml of deionized water then heated for 20 minutes at 60 °C and filtered. Finally, it was transferred to 250 mL Erlenmeyer flask.

2.2. Preparation of pure ZnO and Ca substitute ZnO nanostructures

To synthesize the ZnO sample, the following steps was employed. First, the brown-colored like a solution was obtained by mixing 100 ml of PGF extract and 0.1moleofzinc (II) nitrate hexahydrate solution. Second, the solution was stirred for 4 to 6 hours at 80°C and finally calcination was done at 700 °C for 2 h, for the production of pure crystalline ZnO nanoparticles [14].

To synthesize the Ca-doped ZnO sample, the following steps was employed. First, mixing 100ml of PGF extract solution to 100ml of zinc (II) nitrate hexahydrate with calcium nitrate tetra hydrate (0.95 moles and 0.05 moles) to get brown-colored solution. Second, the solution was stirred for 4 to 6 hours at 80°C and finally calcination was done at 700 °C for 120 minutes as a result in the development of nanomaterials Ca-doped ZnO nanoparticles [14]. The prepared ZnO and Ca-doped ZnO samples are labeled ZNP and CZNP, respectively.

2.3. Characterization

An X-ray diffractometer (model: X'PERT PROP Analytical) was used to examine the produced samples. The diffraction patterns of synthesized materials in the 20°-80° range were recorded using a λ = 1.54Å monochromatic light. An FEI-QUANDA 200F microscope at 30 kV was used to perform HRSEM with EDAX is used for elemental composition. Bruker RFS 25 spectrometer was used to record FT-Raman spectra. A JOVIN YVON FLUROLOG-3-11 spectrometer was used to analyze photoluminescence (PL) 450-600 nm wavelength range. A TGA Q500 U20.10 Build 36 thermal analyzer was used to measure the TG-DTA of synthesized samples. A PMC Micro Mag 3900 type VSM equipped with a 1 T magnet is used to study magnetization curves at room temperature.

2.4. Antibacterial Activity

The antimicrobial activity of ZNP and CZNP nanoparticles was examine during the agar well diffusion method. This was carried out in accordance with Clinical and Laboratory Standards Institute against gram-positive (S. aureus, S. pneumonia) and gram-negative (K. pneumonia, E. coli) pathogenic bacterial strains on Muller-Hinton agar. The media plates was streaked with bacteria 2-3 times and then rotated at 60 °C angles for each streak in order to maintain the uniformity of the mixture. S. aureus, S. pnemoniae, K. pneumoniae, and E. coli overnight cultures in 100 mL were swabbed onto the agar plates using a sterile L-shaped glass rod. Wells of depth 6 mm were made in each petri dish using a sterilized corkborer. The petri plates were then filled with ZNP and CZNP (1 mg for both gram-positive and gram-negative microorganisms). The plates were kept at 37 °C for 1 day to allow bacteria to grow. The diameter of the zone of inhibition was measured after the incubation period. To examine the efficacy of the test samples, a standard antibiotic (Amoxicillin) was utilized as a positive control against human pathogens.

3. Results and discussion

3.1.XRD analysis

The diffraction patterns of ZnO and Ca-substituted ZnO nanoparticles were recorded in the 2θ range between 20° to 80° at room temperature using X-ray diffractometer (Fig. 1a).The X-ray diffraction peaks exhibit hexagonal wurtzite structure, which is well-matched with JCPDS Card No. 79-2205. There is no impurity phases are observed, implying that ZnO structure is not disturbed by doping calcium ions [15].

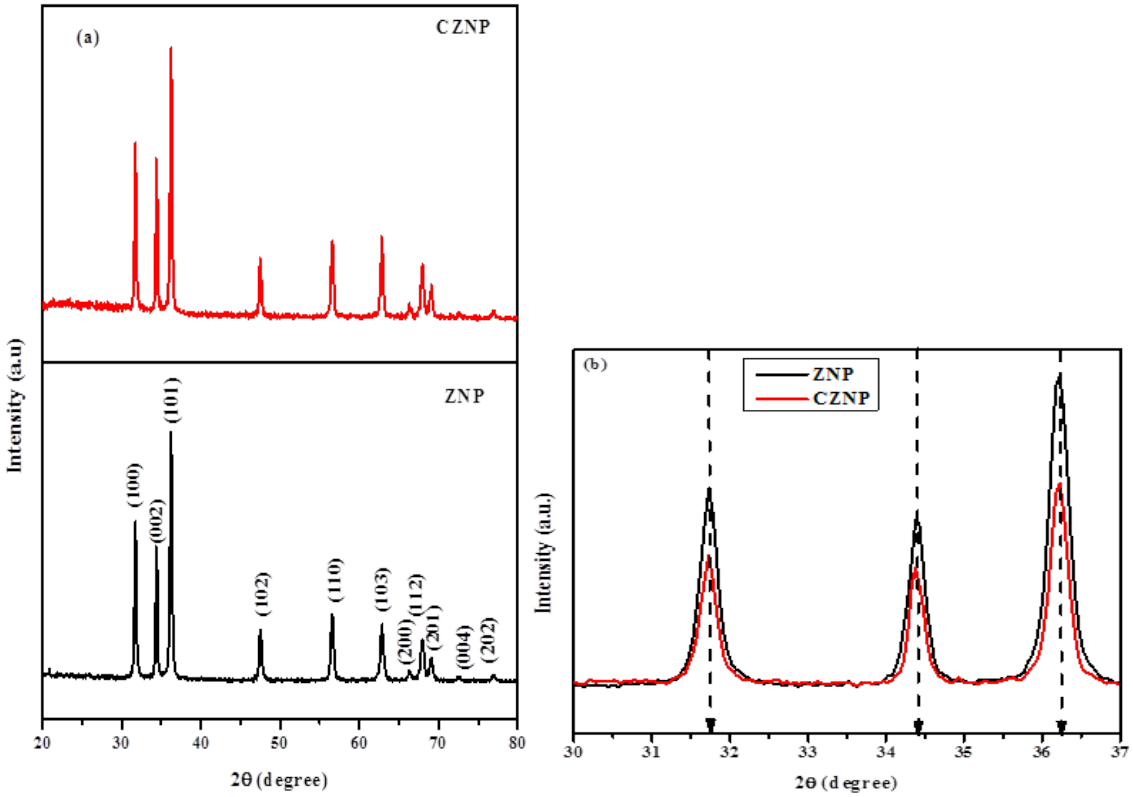

Fig. 1. (a-b).X-ray diffraction pattern of ZNP and CZNP samples.

The XRD peaks of pure ZNP and CZNP samples under investigations were indexed using Bragg's law. The prominent Bragg reflections planes of pure ZNPs were observed at 2θ values are 31.68°, 34.36° and 36.18° which are assigned to be (100), (002) and (101) crystallographic planes. Besides, the peaks observed at 2θ values are 31.66°, 34.34° and 36.16° correspond to the (100),

(002) and (101) Braggs reflection planes of CZNPs [17]. The lattice parameter of ZnO and Ca substituted ZnO nanoparticles were calculated based on the X-ray diffraction patterns using eqn. (1).

$$\frac{1}{d^2} = \frac{4}{3}\left(\frac{h^2 + hk + k^2}{a^2}\right) + \frac{l^2}{c^2} \tag{1}$$

where the lattice constants are *a (b), c*, and *d* is the lattice constants. Fig. 1b displayed the maximum intensity diffraction peaks shift toward a lower angle as the doping Ca^{2+}, which indicating that the lattice constant a and c are increased from3.248 to 3.250 Å and 5.205 to 5.211 Å. This lattice expansion can be caused by the partial substitute of larger ionic radius of r_{Ca}^{2+} = 0.099 nm by the smaller ionic radius r_{Zn}^{2+} = 0.074 nm. On the other hand, substitution of calcium by zinc site changes the ionic radius and causes variations in interatomic distance ('d') resulting in a lower angle shift [18].

The average nano-crystalline of the pure ZNP and CZNP samples are evaluated from the Debye–Scherrereqn. (2) [19, 20] as follows,

$$D = \frac{k\lambda}{\beta \cos\theta} \tag{2}$$

where *k* is a constant of 0.89, X-ray source wavelength (λ) is 0.15406 Å, and diffraction angle (θ) follows Bragg's law, β is a diffraction peaks were prepared nanomaterials in full with half maximum. Scherrer's equation revealed that for pure ZNPs and CZNPs, the average crystallite size was 40 nm and 37 nm, respectively [21, 22] which confirms the nanometer dimensions of the synthesized nanoparticles. Also, from the evaluation it was found that the average crystalline size of CZNP sample is less when compared to ZNP sample. The growth and nucleation of major material (ZNP) was controlled by the dopant Ca^{2+}ions, due to this reason CZNP samples size decrease [23, 24].

3.3. HR-SEM and EDX analysis

The surface morphology of both ZnO and Ca substitute ZnO nanoparticles is shown in Fig. 2(a-b) as it develops. The synthesized nanoparticles have the formation of nano-grains with nano-flakes and/or flower like nanostructures which were revealed using SEM study. The HR-SEM images was used to compute the grain sizes of the ZNP and CZNP nanoparticles, which were found to be 57 nm and 47 nm, respectively. The grain size of doped nanoparticles was decreasing compared to pure nanoparticles, which is due to Ca^{2+} ion distortion on the ZnO surface when doping. Also, it is evident that the grain sizes are lightly variant from X-ray diffraction, as the HR-SEM is related to aggregate clusters size and the XRD is related domain size in ZNP and CZNPs. The element composition of ZNP and CZNP samples was analyzed using energy dispersive X-ray (EDX) analysis and is shown in Fig. 2c and d. The zinc (Zn), calcium (Ca), and oxygen (O) peaks were confirmed in the figures to be present in the ZNP and CZNP samples, and Table 1 provided the elemental composition of atomic and weight percentage.

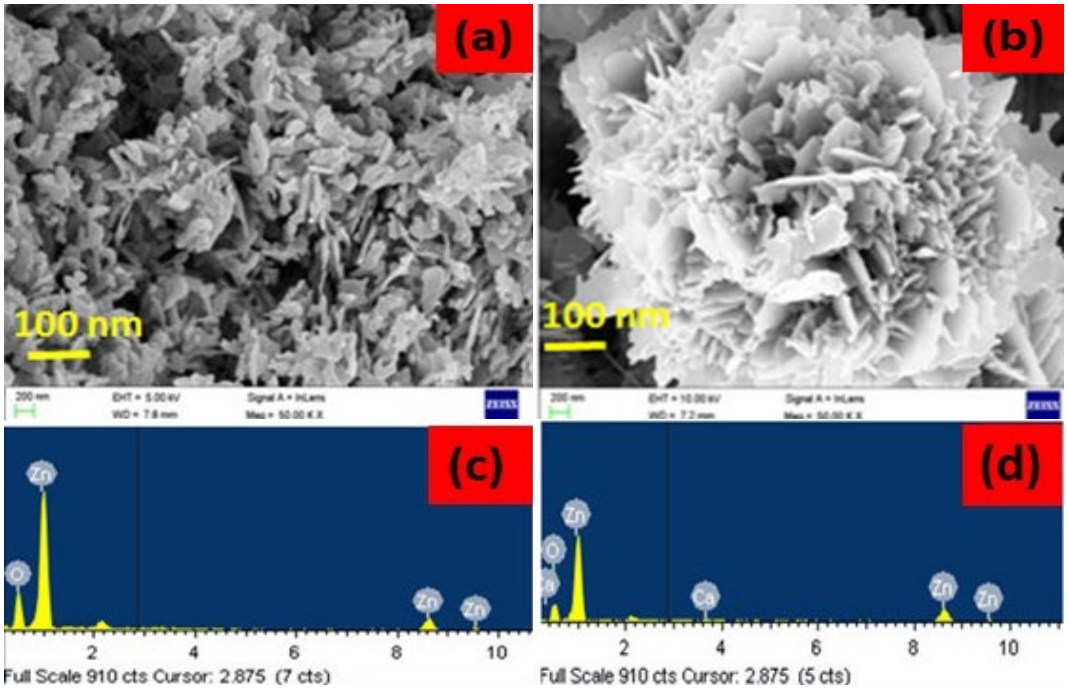

Fig. 2. (a-b).FESEM image of ZNP and CZNP and (c-d) EDAX spectra of ZNP and CZNP samples.

Table 1. The elemental composition of ZNP and CZNP samples.

Sample Code	Percentage (%)			
	Zn	O	Amount of doping	Total
ZNP	43.34	56.66	-	100%
CZNP	44.42	53.66	1.92 (Ca)	100%

3.3. Fourier Infrared Raman spectroscopy studies

Raman spectroscopy can be used to study the photon and phase transition peripheries. Fig. 3(a-b) depicts the wavenumber vs. Raman intensity graphs of ZNP and CZNP samples. Each of the four atoms in a simple ZnO cell occupies the C3v site. As a result, there are 12 phonon branches (nine optical and three acoustic). ZnO NPs have a phonon dispersion relation with 12 branches, which may be decomposed into the following phonon modes using group-theoretical analysis at the Brillouin zone center (q=0).

$$\Gamma = 2(A_1+B_1+E_1+E_2)$$

Among them there are acoustic modes with Γacous. = A_1+E_1 and optical modes with Γopt. = $A_1+2B_1+E_1+2E_2$.

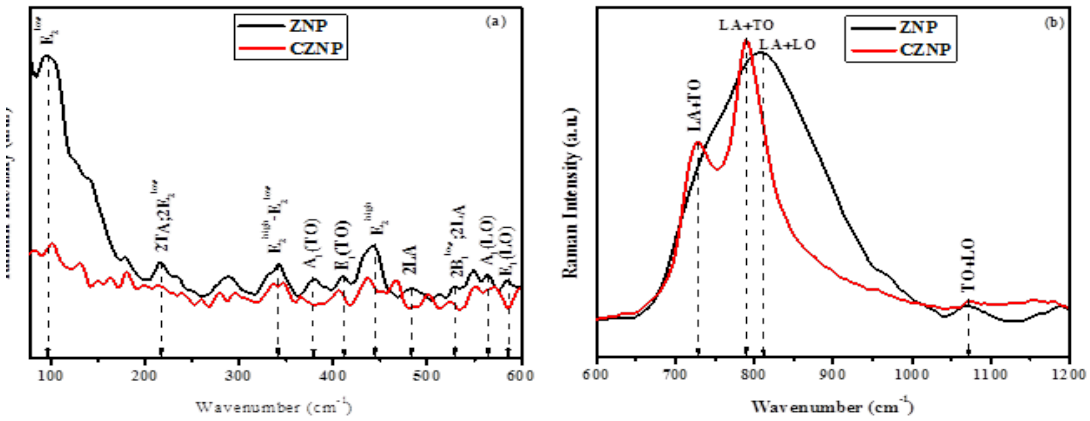

Fig. 3. (a-b).FT-Raman spectra of ZNP and CZNP samples.

The B_1 mode is silent, whereas the others are Raman active. The two splits of phonons with A_1 and E_1 symmetry of polar phonons are TO (transverse optical) and LO (longitudinal optical). Raman and IR activity is the phonon modes A_1 and E_1. The two non-polar mode vibration phonons of E_2 are E_2^{low} and E_2^{high}. The vibrations of the heavy Zn sub-lattice are related to the lower frequency mode E_2 and the higher frequency mode E_2, which are both related to oxygen atoms. Infrared is inactive, and Raman is active in the E_2 non-linear mode. The Raman modes are listed in Table 1. Due to vibration of the Zn sub-lattice in ZNP, the ZNP peak detected at 98 cm^{-1} corresponds to E_2^{low}. However, due to the inclusion of Ca^{2+} ions on the ZnO matrix, CZNP has a slight shift (102 cm^{-1}). The other Raman mode, E_2^{high}, identified in ZNP and CZNP samples at 443 and 445 cm^{-1}, was primarily attributed to oxygen vibrations. The lattice disorder and harmonic phonon-phonon interactions are responsible for their high asymmetry [17]. The A_1 (LO) mode for ZNP and CZNP samples at 564 and 571 cm^{-1} and the E_1 (LO) mode for ZNP and CZNP samples at 584 and 598 cm^{-1} have relatively comparable wave numbers and increase from the background, which is caused by 2nd order Raman scattering. The presence of Ca impurities or imperfections can have an impact on both this mode and the E_1 (LO) mode. This is due to the effect of phonons outside the Brillouin Zone's core. The discrepancy between E_2^{high}-E_2^{low} is attributed to the low wavenumber area of the 2nd order Raman mode at 341 and 346 cm^{-1}.

The 2nd-order aman modesforA_1 symmetry such as 482, 810, 467,728 and 789cm^{-1}were ZNP and CZNP samples. The CZNP samples have some small shift due to Ca^{2+} ions in ZnO matrix, so that reason lattice disorder obtains in ZNP samples. Raman peak at 1000cm^{-1}described to the overtones and/or combination bands. In CZNP samples, Phonon absorption bands are washed-out due to Ca^{2+} ions decrease the spin phonon interaction constant through induced tensile stress [21-24].

3.4. Optical properties

Fig. 4 shows the optical band gap of ZNP and CZNP samples were evaluated by diffuse reflectance spectroscopy. Diffuse reflectance is typically converted into similar absorption coefficients over the equation (4) using the Kubelka-Munk (K-M) function in order to derive the optical band gap as modified Tau'c eqn. (3) and the powder samples[25-27].

$$\alpha h\upsilon = A(h\upsilon - E_g)^a \quad (3)$$

$$F(R) = \alpha = \frac{(1-R)^2}{2R} \quad (4)$$

where,

α – absorption coefficient,

h – Planck's constant,

$F(R)$ – kubelka - Munk function,

R – reflectance,

A – constant,

E_g – direct transitions of optical band gap

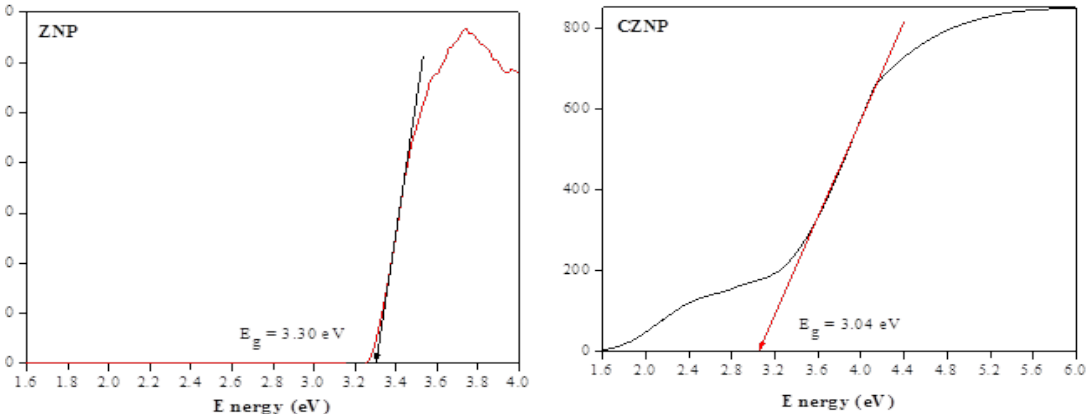

Fig. 4. $(F(R)hv)^2$ versus energy (hv) ofZNP and CZNP samples.

The band gap values are obtained via extrapolating the linear region to the K-M function, which is equal to zero, on a graph between the K-M function vs energy. The optical band gap value of ZnO nanoparticle is found to be 3.30 eV, which is lower than the earlier reported value 3.36 eV, due to quantum confinement effect. Then, the optical band gap decrease (3.04 eV) as Ca^{2+} doping, due to the localized '*d*' electrons are exchange interactions between *sp-d* shell [28].

3.5.TG analysis

The TG curve for ZNP and CZNP samples is shown in Fig. 5, recorded in the temperature range of 30–800 °C in a nitrogen atmosphere. 5.6% weight loss and 5.8% weight loss are observed for ZNP and CZNP samples. Due to water evaporation on the surface of synthesized samples, weight loss occurs.

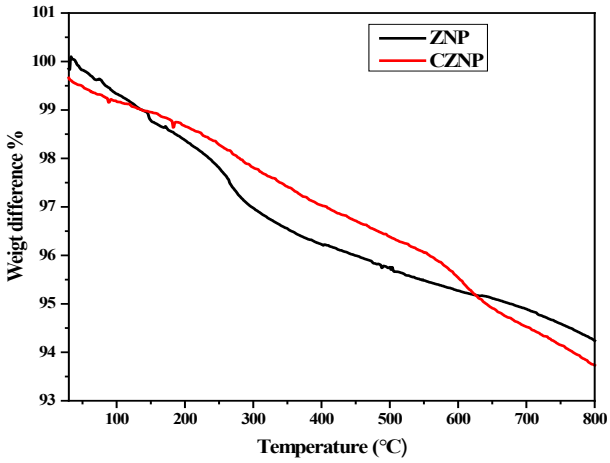

Fig. 5.Thermal gravimetric analysis of ZNP and CZNP samples.

3.6. Magnetic properties

The magnetism of zinc oxide and calcium doped zinc oxide crystal were measured through VSM analysis and results of magnetization (emu/g) versus applied field (KOe) are shown in Fig. 6. From this graph zinc oxide and calcium doped zinc oxide samples exhibit diamagnetic behavior. The coercivity value is 225.11 Oe and then decreases to 142.27 Oe, which is due to the calcium doping with zinc oxide. Further, M_r and $M_s$values decreased from 6.90 to 4.35 memu/g and 0.35 to 0.27 emu/g, respectively. The observed drop in magnetization values is caused by magnetic super exchange interactions, lattice defects and random magnetic orientation. The low retentivity and magnetic saturation may be magnetically clean materials and formation of defects. The current system, diamagnetic behavior caused by the effect of surface size, and oxygen vacancy as a crucial element [29].

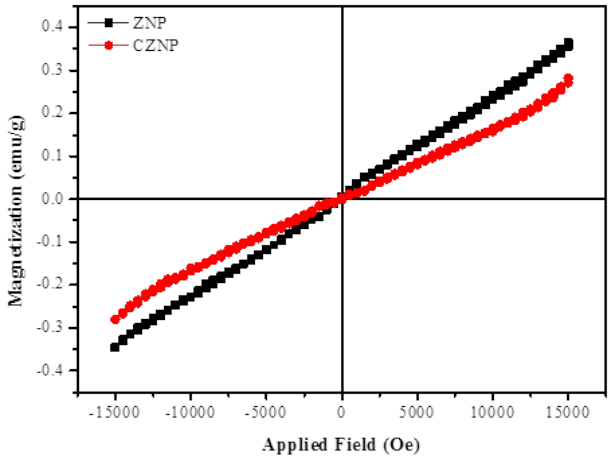

Fig. 6. Magnetic hysteresis curves of ZNP and CZNP nanoparticles.

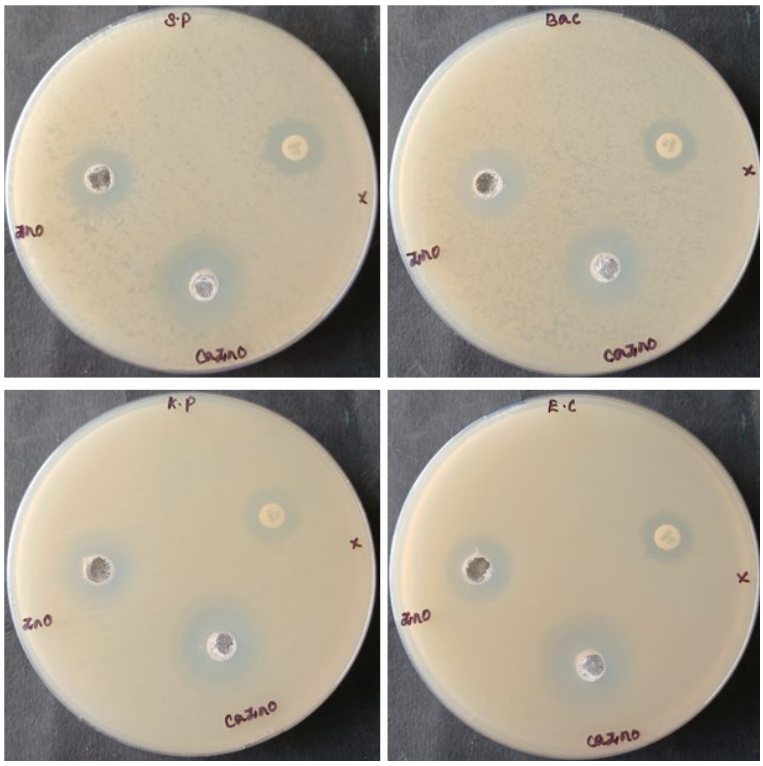

Fig. 7. Antibacterial activity of ZNP and CZNP tested again gram positive and gram negative bacteria's.

3.7. Antibacterial activity

The green synthesis of ZNP and CZNP was tested against gram-positive bacteria (*S. aureus and B. subtilis*) and gram negative bacteria (*K. pneumonia* and *E. coli*) strains by the agar well diffusion method as shown in Fig. 7. The ZNP and CZNP exhibit more antibacterial activity than the Amoxicillin (standard antibiotic) pharmaceutical formulation. The mechanism of ZnO NP's antibacterial action is still being debated. A ZnO nanoparticle's ability to produce reactive oxygen species (ROS) such as O_2, HO_2, and H_2O_2, which can destroy cellular components like DNA, proteins, and lipids, is one of the most well-known antimicrobial activity mechanisms [30, 31]. Also, the oxidative stress inside the bacterial cell was seen which may be due to higher number of oxygen vacancies, the potential of reactant molecules to diffusion (doping of Ca^{2+}), and the release of Zn^{2+} ions.

As a result, producing reactive oxygen species (ROS) is strongly promoted. PL tests show a higher number of oxygen vacancies (O_v) at 551 nm for CZNP compared to 545 nm for ZNP which is because of the increased number of ROS created in the CZNP samples. [30, 31]

4. Conclusion

In summary, the ZNP and CZNP samples were synthesized using PGF extract by green synthesis method. The synthesized nanoparticles showed hexagonal wurtzite structures was confirmed from the XRD studies. The average crystallite size for samples of ZNP and CZNP was revealed to be 40 nm and 37 nm, accordingly. In HR-SEM images showed that the nano-sized crystallized grains with nano-flakes and/or flower like nanostructures. The Raman spectra, E_2^{high} mode was observed at 443 & 445cm^{-1} dominantly assigned to the vibrations of oxygen for ZNP and CZNP samples and which was asymmetry ascribed to the lattice disorder, and also a harmonic phonon-phonon interactions. The optical band gap was found to be 3.30 eV for ZNP and 3.04 eV for CZNP nanoparticles. The weight loss of samples due to the evaporation of water on the surface used thermogravimetric analysis.

The Magnetization–Field (M–H) hysteresis curves revealed the appearance of diamagnetic behavior at room temperature. Subsequently, the pure ZNP and CZNP samples were investigated for superior antibacterial activity. The comparison of two metal-oxides, the CZNP (Ca-doped ZnO) sample exhibit potential antibacterial activity against human pathogens.

Acknowledgements

The author (R.J) acknowledge the financial support through Researchers Supporting Project number (RSP2023R354), King Saud University, Riyadh 11451, Saudi Arabia.

References

[1] N. Sharma, S. Granville, S. C. Kashyap, Phys. Rev. B 82, 125211; https://doi.org/10.1103/PhysRevB.82.125211

[2] J Alaria, P Turek, M Bernard, M Bouloudenine, A Berbadj, N Brihi, G Schmerber, S Colis, A Dinia, No ferromagnetism in Mn doped ZnO semiconductors, 414 (2005) 337-41; https://doi.org/10.1016/j.cplett.2005.09.003

[3]Ghusoon M Ali, P Chakrabarti, ZJ. Phys. D: Appl. Phys. 43 (2010) 415103; https://doi.org/10.1088/0022-3727/43/41/415103

[4] M. H. Sluiter, Y. Kawazoe, P. Sharma, A. Inoue, A. R. Raju, C. Rout, U. V. Waghmare, Phys. Rev. Lett., 94 (2005) 187204; https://doi.org/10.1103/PhysRevLett.94.187204

[5] M. Agila, S. Krithiga, Int. J. Eng. Sci. Manag. Res. 2 (2) (2019) 475-482.

[6] M. Sukumar, L. John Kennedy, J. Judith Vijaya, B. Al-Najar, M. Bououdina, Ceram. Int. 44 (2018) 18113-18122; https://doi.org/10.1016/j.ceramint.2018.07.017

[7] A.S.H. Hameed, C. Karthikeyan, A.P. Ahamed, N. Thajuddin, N.S. Alharbi, S.A. Alharbi, G. Ravi, Sci. Rep. 6 (2016) 24312; https://doi.org/10.1038/srep24312

[8] M. Sundararajan, J. Vidhya, R. Revathi, M. Sukumar, B. Arunadevi, R. Rajkumar, S. Ramachandran, M. Kamalakannan, Chandra Sekhar Dash, JothiRamalingamRajabathar, SelvarajAroykaraj, Inorg. Nano-Met. Chem.; https://doi.org/10.1080/24701556.2021.2025400

[9] B. Chavillon, L. Cario, A. Renaud, F. Tessier, F. Cheviré, M. Boujtita, Y. Pellegrin, E. Blart, A. Smeigh, L. Hammarstrom, F. Odobel, J. Am. Chem. Soc., 134 (2011) 464-70; https://doi.org/10.1021/ja208044k

[10] Shashi B. Rana, Amarpal Singh &NavneetKaur, J. Mater. Sci. Mater. Electron, 24 (2013) 44-52; https://doi.org/10.1007/s10854-012-0795-5

[11] D.C. Look, Mater. Sci. Eng. B, 80 (2001) 383-387; https://doi.org/10.1016/S0921-5107(00)00604-8

[12] Chandra Sekhar Dash, Jothiramalingam Rajabathar, Hamad Al-Lohedan, SelvarajArokiyaraj, S. Ramachandran, M. Sukumar, R. Revathi, G. Anitha, M. Sundararajan, Inorg. Nano-Met. Chem.; https://doi.org/10.1080/24701556.2022.2034017

[13] M Schumm, M Koerdel, S Müller, H Zutz, C Ronning, J Stehr, D M Hofmann, J Geurts, New J. Phys.10 (2008) 043004; https://doi.org/10.1088/1367-2630/10/4/043004

[14] J. Lang, J. Wang, Q. Zhang, X. Songsong, Q. Han, Y. Zhang, Hongju. Zhai, J. Cao, Y. Yan, J. Yang, Chem. Res. Chin. Univ. 30 (2014) 538-542; https://doi.org/10.1007/s40242-014-4028-8

[15] A. Bechen, M. Durr, L.P. Nostro, P. Baglioni, J. Nanoparticle Res. 10 (2008) 679-689; https://doi.org/10.1007/s11051-007-9318-3

[16]OnyekachiKalu, I Ahemen, Hilda Esparza Ponce, José Alberto Duarte Moller, A Reyes Rojas, J. Phys. D: Appl. Phys. 54 345108; https://doi.org/10.1088/1361-6463/ac021c

[17] Hidetoshi Arima, Gen-ichiDanno, Biosci. Biotechnol. Biochem. 66 (2002) 1727-1730; https://doi.org/10.1271/bbb.66.1727

[18]SumraNaseer, ShabbirHussain, NaureenNaeem, Muhammad Pervaiz, MadihaRahman,

Clin.Phytosci. 4, 32 (2018); https://doi.org/10.1186/s40816-018-0093-8

[19] M. Sukumar, M. Agila, A. Sutha, V. Ravi, Abdullah M. Al-Enizi, MohdUbaidullah, Mohammad Shahzad Samdani, M. Sundararajan,Bidhan Pandit, J. Mater. Sci.: Mater. Electron. 33 (35), 26144-26156; https://doi.org/10.1007/s10854-022-09301-7

[20] K. Samanta, P. Bhattacharya, R. S. Katiyar, W. Iwamoto, P. G. Pagliuso, C. Rettori, Rev. B 73, 245213.

[21] M. Sukumar, L. John Kennedy, J. Judith Vijaya, B. Al-Najar, M. Bououdina, GopinathMudhan, Vacuum 167 (2019) 407-415; https://doi.org/10.1016/j.vacuum.2019.06.036

[22] T David, S Goldsmith, R L Boxman, J. Phys. D: Appl. Phys. 38 (2005) 2407; https://doi.org/10.1088/0022-3727/38/14/017

[23] Chandrasekaran Karthikeyan, KokkarachedduVaraprasad, Ali Akbari-Fakhrabadi, Abdulrahman SyedahamedHaja Hameed, Rotimi Sadiku, Carbohydr. Polym, 249 (2020) 116825; https://doi.org/10.1016/j.carbpol.2020.116825

[24] S. Kanithan, N. ArunVignesh, KhadijahMohammedsalehKatubi, ParthaSarathiSubudhi, EkremYanmaz, JoshuvaArockiaDhanraj, Norah Salem Alsaiari, Khamael M. Abualnaja, M. Sukumar, M. Sundararajan, S. Baskar, SrikantaSahu, Chandra Sekhar Dash, J. Mol. Struct. 1265 (2022) 133289; https://doi.org/10.1016/j.molstruc.2022.133289

[25] K. Mathankumar, M. Sukumar, Chandra Sekhar Dash, M. Sundararajan, MohdUbaidullah, Abdullah M. Al-Enizi, A. Sutha, Md. KausarRaza, JoshuvaArockiaDhanraj, Dinesh Kumar, J.Inorg.Organomet.Polym. Mater., 32 (2022) 3476-3487; https://doi.org/10.1007/s10904-022-02382-1

[26] M. Sundararajan, A. Subramani, MohdUbaidullah, Shoyebmohamad F. Shaikh, Bidhan Pandit, S. K. Jesudoss, M. Kamalakannan, S. Yuvaraj, ParthaSarathiSubudhi, Chandra Sekhar Dash, Synthesis, J. Clust. Sci 33 (2022) 1821-1830; https://doi.org/10.1007/s10876-022-02239-0

[27] M. Sundararajan, M. Sukumar, Chandra Sekhar Dash, A. Sutha, S. Suresh, MohdUbaidullah, Abdullah M. Al-Enizi, MdKausarRaza, Dinesh Kumar, Phys. B: Condens. Matter. 644 (2022) 414232; https://doi.org/10.1016/j.physb.2022.414232

[28]ManickamMinakshi, David R. G. Mitchell, Christian Baur, Johann Chable, Anders J. Barlow, Maximilian Fichtner, Amitava Banerjee, Sudip Chakraborty, Rajeev Ahuja, Nanoscale Adv., 2019, 1, 565; https://doi.org/10.1039/C8NA00156A

[29] Ibrahim M. Maafa, Abdullah M.Al-Enizi, Ahmed Abutaleb, Nasser I. Zouli, MohdUbaidullah, Shoyeb Mohamad F. Shaikh, Mohammed A. Al-Abdrabalnabi, AymanYousef, Alex. Eng. J., 60 (2021) 1819-1826; https://doi.org/10.1016/j.aej.2020.11.030

[30] M. Ponnar, C.Thangamani, P.Monisha, S.S.Gomathi, K.Pushpanathan, Applied Surface Science., 449 (2018) 132-143; https://doi.org/10.1016/j.apsusc.2018.01.126

[31] K. Ravichandran, A. JansiSanthosam, Omar M. Aldossary, MohdUbaidullah, Phys. Scr., 96 (2021) 125825; https://doi.org/10.1088/1402-4896/ac2545